Possibility-based multidisciplinary optimisation for electric-powered unmanned aerial vehicle design

N. V. Nguyen
nhuvan@gmail.com

J.-W. Lee
jwlee@konkuk.ac.kr

M. Tyan

Aerospace Information Engineering
Konkuk University
Seoul
South Korea

D. Lee

LIG Nex1
PGM R&D Center
South Korea

ABSTRACT

This paper describes a possibility-based multidisciplinary optimisation for electric-powered unmanned aerial vehicles (UAVs) design. An in-house integrated UAV (iUAV) analysis program that uses an electric-powered motor was developed and validated by a Predator A configuration for aerodynamics, weight, and performance parameters. An electric-powered propulsion system was proposed to replace a piston engine and fuel with an electric motor, power controllers, and battery from an eco-system point of view. Moreover, an in-house Possibility-Based Design Optimisation (iPBDO) solver was researched and developed to effectively handle uncertainty variables and parameters and to further shift constraints into a feasible design space. A sensitivity analysis was performed to reduce the dimensions of design variables and the computational load during the iPBDO process. Maximising the electric-powered UAV endurance while solving the iPBDO yields more conservative, but more reliable, optimal UAV configuration results than the traditional deterministic optimisation approach. A high fidelity analysis was used to demonstrate the effectiveness of the process by verifying the accuracy of the optimal electric-powered UAV configuration at two possibility index values and a baseline.

Paper No. 4138. Manuscript received 9 February 2014 and accepted 28 May 2015.

https://doi.org/10.1017/S0001924000011313 Published online by Cambridge University Press

NOMENCLATURE

ΔC_{dflap}	increase drag due to flap deflection
C_{Do}	parasite drag coefficient
C_{Di}	induced drag coefficient
C_L	lift coefficient
C_{Lmax}	maximum lift coefficient
$C_{l\beta}$	static lateral derivative
$C_{m\alpha}$	static pitching derivative
$C_{n\beta}$	static directional derivative
C_T	thrust coefficient
h	flight altitude, m
J	propeller advanced ratio
k	induced drag factor
L/D	lift to drag ratio
PCT	power setting, %
R/C	rate of climb, ms^{-1}
S_{to}	take-off distance, m
S_{tand}	landing distance, m
S_W	wing area, m^2
V_{stall}	stall speed, ms^{-1}
V_{max}	maximum speed, ms^{-1}
V_{design}	design flight speed, ms^{-1}
W_e	empty weight, kg
W_o	take-off gross weight, kg
α	possibility index
β	propeller pitch angle
η_{prop}	propeller efficiency
η_m	motor efficiency

Acronyms

CFD	Computational Fluid Dynamics
HT	Horizontal Tail
MALE	Medium Altitude Long Endurance
RDO	Robust Design Optimisation
RBDO	Reliability Based Design Optimisation
PBDO	Possibility Based Design Optimisation
SM	Static Margin
UAV	Unmanned Aerial Vehicle
VT	Vertical Tail
WOT	Wide Open Throttle

1.0 INTRODUCTION

Recently, aircraft conceptual design has aimed to develop or implement quick and accurate design analysis tools to seek the deterministic optimal design solutions by compromising many complex and highly coupled subsystems and disciplines[1] with the help of optimisation algorithms. The optimal

https://doi.org/10.1017/S0001924000011313 Published online by Cambridge University Press

results from the conceptual design stage play an extremely important role in the next preliminary and detailed design stages. However, the nondeterministic nature of the complex aircraft design problem and the importance of modelling the human designer's decision-making activities have been largely neglected at the conceptual design stage[2]. For example, the design flight speed is required as a design variable to maximise the critical performance features of the aircraft for the conceptual design of a MALE UAV. The design flight speed might be slightly changeable during very long endurance tests or it might be affected by the wind or flight altitude. In addition, the round off of main geometry parameters during the construction of the mathematical models or the manufacturing stage and the lack of knowledge might lead to variations in the conceptual optimal design solutions. These sources are referred to as the uncertainty or unexpected derivations. Design optimisation under uncertainty extends traditional design optimisation methods by integrating uncertainty modelling to predict the influence of uncertain variables or parameters on a solution, which yields more conservative designs. Three disciplines have emerged to address designs with uncertainty: Reliability-Based Design Optimisation (RBDO), Possibility-Based Design Optimisation (PBDO)[3], and Reliability-Based Robust Design Optimisation (RBRDO[4,5]. Both RBDO and PBDO are optimisation strategies that enforce the desired likelihood that constraints will be satisfied when the design is fabricated and tested or subjected to more reliable analysis methods. RBDO utilises probabilistic modelling to represent uncertain quantities. PBDO was developed for problems that contain sources of uncertainty and that lack the knowledge or data to build accurate probability models. These methods are applied to prevent such phenomena[6]. Wet Chen *et al* applied the Robust Design Optimisation (RDO) to improve the handling performance of vehicles. RDO is effective to prevent the worst manoeuvre condition as well as a range of manoeuvre inputs[7]. Daniel *et al* also applied RBDO to an aircraft conceptual design and wing box design optimisation[8,9].

In addition, global warming has been raising average temperatures and sea levels around the world, and extreme weather phenomenon and ecological destruction have been causing changes across our lives at a rapid pace. The aviation industry emitted approximately 600million tons of CO_2 as of 2007 and is expected to be responsible for 15% of the total global CO_2 emissions by 2050 [10]. However, the emissions of pollutants can be fundamentally addressed by using electricity as the main source of power instead of fossil fuels. Moreover, the control bandwidth available to the motor can conceivably be used improve the roll axis stability for sensing and targeting. Furthermore, electric aircraft are already under development in a number of countries, even though the options for improving the performance of internal combustion are limited[11]. The Taurus Electro (G2) from Pipistrel, Slovenia and E430 from Yuneec, China have already entered the commercialisation stage, while Electra – one from PC-Aero and Antares 20E glider from Lange Aviation, Germany are under development[12,13].

Conversely, electric-powered UAVs have not yet entered the commercialisation stage. However, many countries are engaged in the study of electric-powered and hybrid UAVs with internal combustion engines, mainly for small-sized engines. Inventus E developed by Lew Aerospace is powered by an electric motor and shows high endurance at high-altitude. UAV Zephyr, developed by QinetiQ in the UK, is now in trials and relies on solar cells and batteries for flights exceeding 80hours in the stratosphere. In addition, research centres, such as DARPA (Defence Advanced Research Projects Agency), Boeing, and IIT (Israel Institute of Technology), are researching hybrid propulsion systems for UAVs that rely on electric power[14].

Currently, many studies are actively examining electric-powered UAVs. However, this technology still shows obvious limitations. The biggest challenges are the battery capacity, regulation, and specification issues. Electric aircraft are currently not subject to regulations or specifications. The ASTM (American Society of Testing Materials) is a standard-setting body that is defining the specifications for LSA (Light Sports Aircraft) aircraft powered solely by electricity, and the FAA (Federal Aviation

https://doi.org/10.1017/S0001924000011313 Published online by Cambridge University Press

Administration) of the US plans to review these specifications for acceptance in the future. The batteries used in electric aircraft need to be certified for overheating protection, waterproofing, charging efficiency, and intelligent self-diagnosis for aviation certification. In addition, batteries that deliver a higher density are required because the energy density of a battery significantly impacts the weight of electric aircraft. Fortunately, battery technologies are expected to advance rapidly due to the growth of electric vehicle technology, which is one step ahead of the development of electric aircraft[13].

The design of an electric-powered UAV was optimised in this study. Specifically, the replacement of a piston engine system by an electric-powered system was studied and integrated into the design and analysis programs of developed UAVs to maximise the endurance of the UAV. However, many uncertainty variables and parameters affect the endurance of an electric-powered UAV, such as the battery voltage, battery capacity, flight altitude, payload, and design speed. Neglecting these parameters in the design process might result in unpredictable design results. Therefore, a design method that implements PBDO was proposed for electric-powered UAVs to obtain more realistic UAV results while considering uncertainty parameters and variables in the design optimisation process. Both the deterministic and PBDO optimum MALE UAV results are presented.

2.0 INTEGRATED ANALYSIS PROGRAM FOR ELECTRIC-POWERED UAVS

An integrated UAV (iUAV) program was developed and validated in MATLAB for the design and analysis of UAVs[15]. The iUAV program is composed of geometry, weight, aero and S&C, propulsion, performance, and mission analysis disciplines, as shown in Fig. 1. These components form the Design Structural Matrix (DSM). The feed-forward parameters are straightforward and sequentially provide the next disciplines.

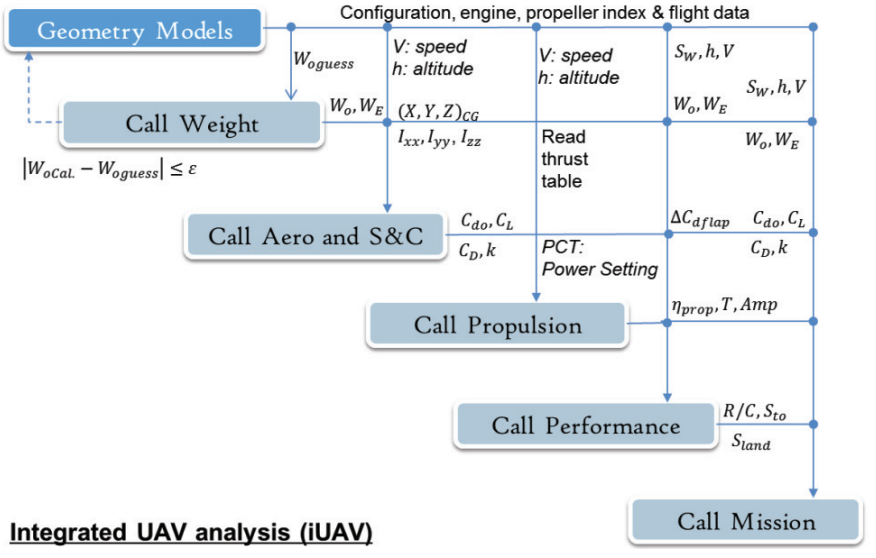


Figure 1. Integrated UAV (iUAV) analysis dataflow.

https://doi.org/10.1017/S0001924000011313 Published online by Cambridge University Press

However, a feedback parameter from the weight analysis discipline is resolved by using a fixed-point iteration method until the solution converges. The gross weight is then used to predict other weight components and provide these data to other disciplines, as shown in Fig. 1.

2.1 Aerodynamics and S&C analysis discipline

The designed Unmanned Aerial Vehicles (UAVs) is a Medium Range and Long Endurance (MALE), which operates at an altitude of approximately 5,000-15,000metres and shows an endurance of 24 hours at low speed. The MALE UAVs feature a long wingspan to maximise the aerodynamic efficiency during surveillance missions that require high resolution and a thermal camera. Hence, the aerodynamic and stability & control (S&C) analysis discipline is required to accurately and quickly estimate the lift and drag for aircraft with a long wing span and low speed unmanned aircrafts at different flight conditions, such as take-off, climb, cruise, descent, loiter, and landing. AVL's Drela code[16], which employs an extended vortex lattice model for the lifting surfaces together with a slender-body model for fuselages and nacelles, was implemented to determine the trim lift coefficient (C_L), induced drag coefficient (C_{Di}), and estimate the S&C. In addition, a maximum lift coefficient (C_{Lmax}) estimation subroutine at take-off and landing conditions was added to the lift analysis discipline for various flap deflection angles. A parasite drag estimation was developed and validated by using semi-empirical equations for aircraft components, namely AERO09[15]. Therefore, the lift coefficient (C_L), maximum lift coefficient (C_{Lmax}), induced drag coefficient (C_{Di}), and parasite drag (C_{do}) were estimated for a given aircraft at the different flight condition and flap configurations. Moreover, the S&C analysis discipline predicted the static and dynamic stability derivatives for a given aircraft.

2.2 Weight analysis discipline

The weight analysis discipline was constructed by implementing the build-up of weight components from Raymer and Roskam[17,18]. However, the piecewise linear beam theory was used to estimate the MALE UAV wing weight due to its long wingspan characteristic[19]. The weight of the subsystems was estimated by calculating the weights of the Flight Control System (FCS), Environmental Control System (ECS), Communication System, Electrical System, and Fuel System. The avionics weight included the Auto Pilot, Inertial Navigation System (INS), Global Positioning System (GPS), Processor, Camera, Recorder, and Air Traffic Control (ATC), which are directly inputted by users. The electric propulsion system was composed of the motor, battery, and power controllers. Each component was assigned a location to predict a centre of gravity. In addition, the inertia moment of the aircraft was estimated for the S&C analysis discipline.

2.3 Electric-powered propulsion analysis discipline

The propeller and electric motor analysis discipline integrates a motor specification database with a propeller aerodynamics solver. The electric motor specifications were obtained from the database and corrected for the temperature and altitude of the specified flight conditions. An optimisation algorithm was used to identify the most efficient propeller angle and throttle setting that produces the correct thrust for an input flight velocity, as shown in Fig. 2. The propulsion analysis discipline was used as an offline analysis to generate a thrust table based on the electric motor and propeller index for the performance and mission analysis at various throttle settings, speeds, and altitudes. The Blade Element Theory (BET) was used to analyse the propeller[20]. An X-foil program[21] was integrated into the BET to estimate the lift and drag coefficients at each propeller blade section. The thrust table includes the speed, available thrust, propeller efficiency, amperage, and propeller optimum blade angle with several tables for various throttle settings.

https://doi.org/10.1017/S0001924000011313 Published online by Cambridge University Press

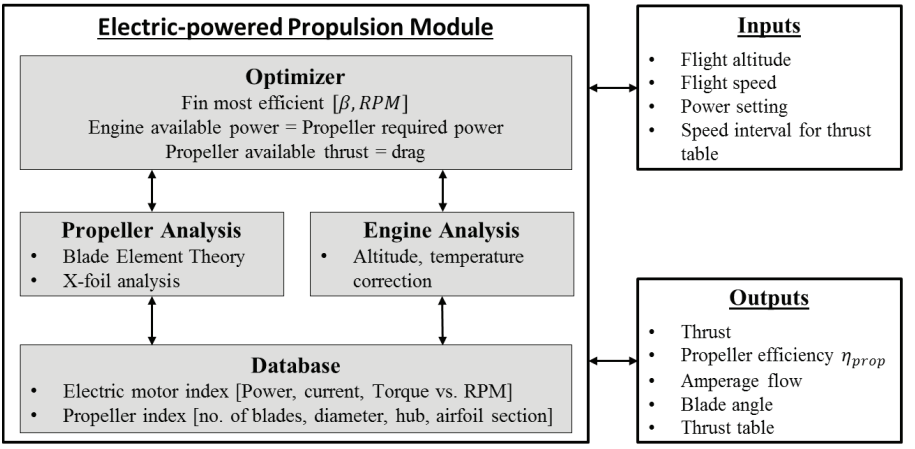


Figure 2. Electric-powered propulsion analysis module.

Table 1
Battery Solutions[13]

	Li Polymer	$FePO_4$	$Li\text{-}SOCl_2$	$Li\text{-}FeS_2$	Lithium – Ion	Nickel – Cadmium
Voltage (V)	3·7	3·2	3·6	1·5	48	4·8
Amp-hours	35	200	19	2·9	45	260
Weight (kg)	1	6·26	0·107	0·0145	23	37
Energy (Watt-hour/kg)	129·5	102·24	639·25	300	93·91	33·73

In addition, a battery was used to provide the power to operate the electric motor. The important factors that influence the selection of the battery are based on the voltage, amperage-hours, weight, and energy for each battery cell for the current and innovative technology. A higher energy or power-to-weight ratio provides more power for same battery weight. Therefore, these ratios are the main criteria to be considered for aerial vehicle applications while ignoring cost considerations. Several battery solutions are listed in Table 1.

2.4 Mission analysis discipline

The mission analysis discipline uses the time simulation method to predict the take-off, landing, climb, descent, loiter, and cruise duration as well as the used amperage during each mission. The equations of motion were derived for each mission to perform the time integration. The used amperage was calculated by multiplying each mission duration with the corresponding amperage in the thrust table[22].

2.5 Performance analysis discipline

The equations of motion were solved for un-accelerated and accelerated flights to determine minimum and maximum speed, maximum rate of climb, turn rate, and service ceiling at different flight altitudes. The take-off and landing time simulation method were applied to determine the take-off and landing distance over obsaatacles or ground roll. In addition, the endurance of an

https://doi.org/10.1017/S0001924000011313 Published online by Cambridge University Press

electric-powered UAV is given by Equation (3), which is affected by the constant weight of an electric-powered UAV based on the battery capacity, motor voltage, required power, and required current as shown in Equations (1) and (2) [19, 22]:

$$\text{The required current: } I_{req} = \frac{P_{req}(W)}{Voltage(V)} \quad \ldots (1)$$

$$\text{Where, the required power: } p_{req} = \frac{T \times V}{\eta} = \frac{T \times V}{\eta_m \times \eta_{prop}} \quad \ldots (2)$$

T is a required thrust, V is an aircraft speed, and η is the propulsion efficiency.
The endurance equation for electric-powered UAV:

$$Endurance = \frac{BatteryCapacity(Amp-Hr) \times \eta_m \times \eta_{prop}}{\frac{1}{2}\rho\left(C_{Do} + k\left(\frac{W}{\frac{1}{2}\rho S_W V^2}\right)^2\right) S_W V^3 / Voltage} \quad \ldots (3)$$

2.6 Possibility Based Design Optimisation (PBDO) solver

Possibility Based Design Optimisation (PBDO) accounts for uncertainties by modelling each source of uncertainty as a fuzzy number[23]. Fuzzy numbers including uncertainty variable x_u and parameter p_u define an interval in which the true value of the uncertain term could lie. The width of the interval is controlled by adjusting the alpha value, which is referred to as the possibility index. The shape and width of the fuzzy number is typically determined by expert experience or by examining any available data relevant to the variable or parameter[24]. Many methods are currently available to handle optimisation problems with fuzzy variables or parameters[25].

This research implements an in-house PBDO solver (iPBDO) written in the MATLAB programming language shown in Fig. 3[26]. The solver implements a sequential solution strategy. The process begins with a full deterministic optimisation using a Sequential Quadratic Programming (SQP) optimiser followed by a reliability assessment phase with the initial variable $x_{i,o}$ and initial search step $s_{i,o}$ as shown in Fig. 3. An anti-optimisation is performed on each constraint to determine the worst possible combination of the uncertain variable and parameter values within the boundaries defined by each fuzzy number. This information is used to further shift the constraints into the feasible design space. A deterministic optimisation is performed using the shifted constraints. This process is repeated until the results converge.

3.0 POSSIBILITY BASED DESIGN OPTIMISATION FOR ELECTRIC-POWERED UAVS

3.1 Electric-powered UAV design process

The PBDO for electric-powered UAVs design process begins by selecting a generic UAV with piston engine system, as shown in Fig. 4. The electric-powered system, which includes the motor, power controllers, and battery weight, was selected to match the power and weight of a piston propulsion

https://doi.org/10.1017/S0001924000011313 Published online by Cambridge University Press

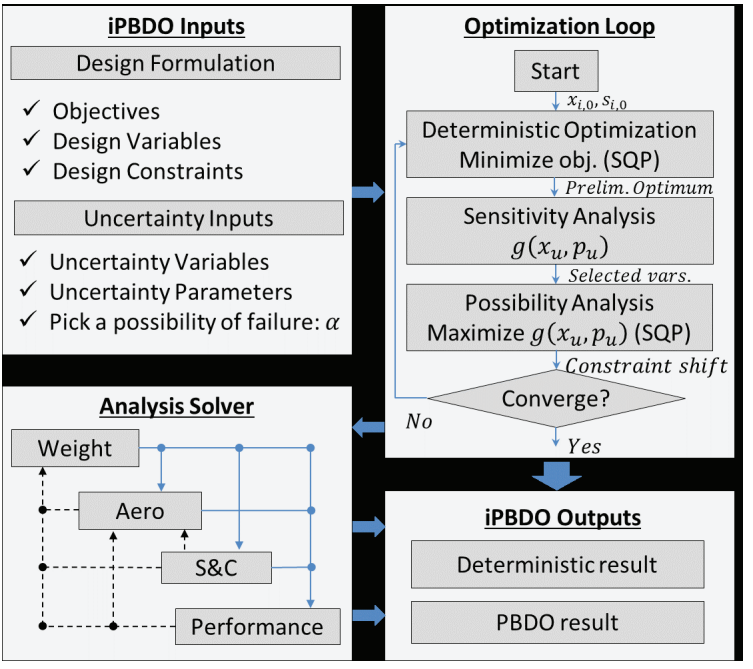


Figure 3. In-house iPBDO solver flowchart.

system. The mission profile, electric-powered system, and UAV baseline configuration data were provided to the iUAV analysis box. A sensitivity analysis was performed to eliminate the small effects of the UAV configuration variables on the performance and other output parameters. The effective variables were then selected as the design variables for the design formulation, as shown in Fig. 4. In addition, the uncertainty consideration was investigated to identify the uncertainty variables that influence the UAV output parameters. Eventually, the iPBDO solver was processed with the help of the design formulation, uncertainty consideration, and iUAV analysis to obtain the optimal UAV configurations with different possibility indices, as shown in Fig. 4. The high fidelity analysis ANSYS Fluent13 was implemented to validate the optimal configuration and baseline[27,28].

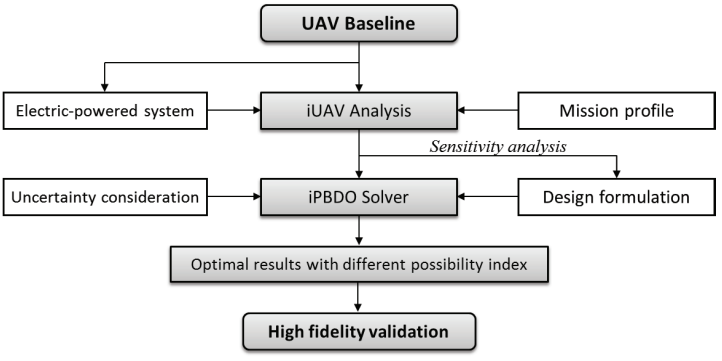


Figure 4. PBDO for electric-powered UAVs design process.

https://doi.org/10.1017/S0001924000011313 Published online by Cambridge University Press

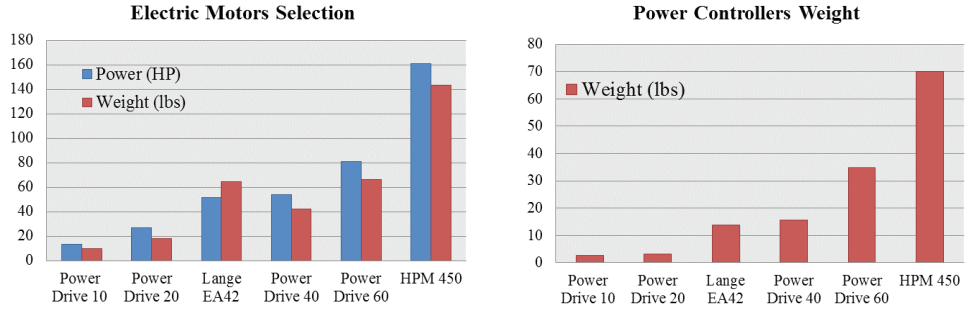


Figure 5. Motors and controllers selections.

3.2 Motor and battery selection for UAV

A Brushless Direct Current (BLDC) has been selected for many aerospace applications due to several advantages, such as a light weight, high efficiency, low noise, and low thermal dissipation[11]. The six BLDC motors ranging from 10HP to 160HP are listed in Fig. 5. The motor and battery systems were selected to replace a Predator A propulsion system, which is a Rotax 115HP turbocharged engine and fuel weight, shown in Fig. 5. The appropriate motor and power controller weight are estimated in Table 4 for a 115HP engine. The power controllers were composed of power controllers and two cable weights, which are shown in Table 2.

Table 2
Selected motor and power controllers

Motor	
Horse Power (HP)	115
Weight (lbs)	98·725
Opt. Voltage (V)	400-700
Power Controllers	
Power Controllers Weight	61·003
Cable (+) (lb)	10
Cable (–) (lb)	10

The electric UAV propulsion system was matched to a Predator A propulsion system at 402·75kg for the propulsion system in Table 3. The battery weight was estimated by using the selected motor and power controller data. Because the Tenergy Li-$SOCl_2$ battery is known to have a very high power-to-weight ratio and light weight[13], it has been used in many aerospace applications[5,6]. Therefore, a Tenergy Li-$SOCl_2$, which has an output of 3·6V, capacity of 19Amp-hours, and weight of 0·107kg per cell, was selected. The electric-powered UAV was assumed to use a 115HP and 600 Voltage motor. Hence, a 100Ah and 600V Tenergy Li-$SOCl_2$ battery pack of 1,755 cells was required to yield a total weight of 188kg. The electric-powered UAV was matched with a 321·25kg battery weight with 3,000 cells of the Tenergy Li-$SOCl_2$ battery.

3.3 Sensitivity analysis

A sensitivity analysis was performed on 21 variables of the MALE UAV configuration, including the wing, horizontal tail, vertical tail, and their locations relative to 17 constraints and the endurance shown in Table 6. Five hundred design points were selected by implementing the Latin Hyper-cube

https://doi.org/10.1017/S0001924000011313 Published online by Cambridge University Press

Table 3
Propulsion system weight for electric UAV

Predator A propulsion system	
Dry engine weight (kg)	75·5
Installed engine weight assumed 10% dry (kg)	7·55
Fuel weight (kg)	301·6
Unused fuel assumed 6% fuel (kg)	18·096
Propulsion system weight (kg)	402·75
Electric UAV propulsion system	
Motor (kg)	44·88
Power controllers (kg)	27·72
Cable (+)	4·45
Cable (-)	4·45
Battery weight (kg)	321·25
Electric UAV propulsion system weight (kg)	402·75

and orthogonal method [27] to execute the iUAV analysis program. Four sensitivity analysis results for the empty weight, stall speed, static margin (SM), and endurance are shown in Fig. 6. The empty weight component is primarily affected by the wing span, design speed, wing geometry, vertical and horizontal tail as shown Fig. 6(a), which agrees with aircraft weight components. Similarly, the static margin is primarily affected by the wing sweep angle (63%), wing x location or wing longitudinal location, and wing root chord, as shown in Fig. 6(c). The wingspan, wing root, and wing tip chord mainly affect the stall speed as shown in Fig. 6(c). The endurance parameter is mainly affected by the design speed (80%) because gross weight is constant for an electric-powered UAV. If the UAV flies at a lower speed, the endurance increases. A combination of the wingspan span speed, which relate to the aerodynamics parameters and other wing geometry parameters, also affect the endurance, as shown in Fig. 6(c). The main variables that affect the UAV endurance and the 17 constraints are shown in Table 6. The wing, vertical tail, and horizontal tail z location or vertical location within 5% effects on objective and 17 constraints are neglected in the design formulation which slightly affected the endurance and constraints. The design altitude is considered as uncertainty parameter.

3.4 Electric-powered UAVs design formulation

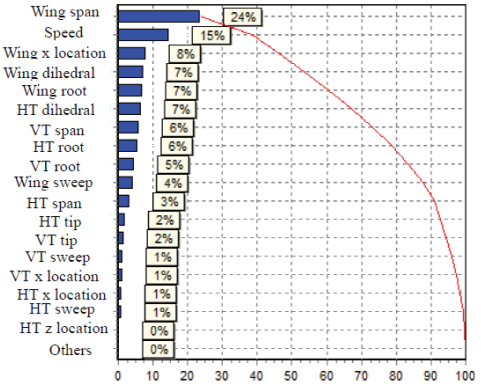
The endurance of a UAVs is a main factor for surveillance and other missions. Therefore, it was selected as an objective function to maximise the endurance of the electric-powered UAV.

$$\textit{Maximise Endurance} = \mathrm{End}(\vec{x_j})\ j = 1, 17 \qquad \ldots (4)$$

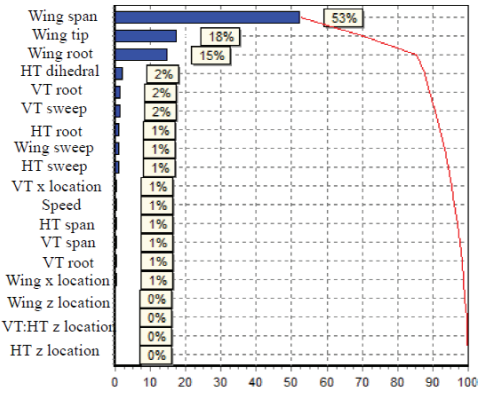
$$\text{Subject to: } \Pi\ (G_i(d(X) > 0)) > \alpha_t,\ \ i = 1, \ldots, 17 \qquad \ldots (5)$$

The 17 design variables are listed in Table 4, including the wing, horizontal tail, vertical tail geometry, and the design speed after sensitivity analysis. The design space for each design variable

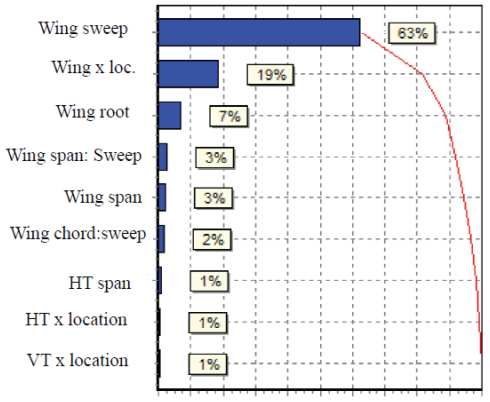
https://doi.org/10.1017/S0001924000011313 Published online by Cambridge University Press



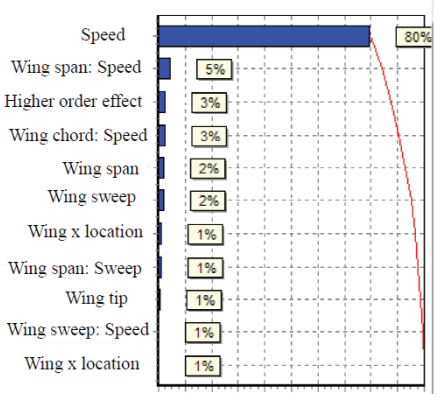
(a) empty weight sensitivity analysis



(b) stall speed sensitivity analysis



(c) SM sensitivity analysis



(d) endurance sensitivity analysis

Figure 6. Sensitivity analysis for electric-powered UAV.

was set at ±25% from a baseline. The lower bound of the design speed variable was set to the stall speed and the upper bound was defined by the maximum speed from the Predator A specifications. The 17 constraints were subjected to geometry, aerodynamics, weight, performance, and S&C analysis parameters, as shown in Table 6. The first run to determine results was executed while satisfying these above constraints. Uncertainty variables were formulated to run the PBDO process, which are shown in Table 5. The design speed was considered an uncertainty variable due to its variability during the course of the mission. The electric-powered propulsion system introduces many uncertainty parameters, which are listed in Table 5. The battery cell and pack were set to their mean value and interval width due to the technology limitations consideration based on engineering experience. In addition, the density correction, design altitude, and propeller efficiency were considered uncertainty parameters due to their effect on the UAV endurance.

https://doi.org/10.1017/S0001924000011313 Published online by Cambridge University Press

Table 4
Design constraints for electric-powered UAV

Constraints	Description	Discipline
G(1)	Static Margin: $SM \geq 0{\cdot}05$	S&C ($@V_{design}$)
G(2)	Static Margin: $SM \leq 0{\cdot}15$	S&C ($@V_{design}$)
G(3)	Take-off field length ≤ 609m (2,000ft)	Perf. (50ft) (*WOT*)
G(4)	Lateral stability derivative: $C_{l\beta} \leq -0{\cdot}03$	S&C ($@V_{design}$)
G(5)	Gross weight: MTOW ≤ 1,020 (kg)	Weight
G(6)	Pitching moment der. $C_{ma} \leq 0$	S&C ($@V_{design}$)
G(7)	Landing distance ≤ 518m (1,700ft)	Performance
G(8)	Empty weight W ≤ 360kg	Weight
G(9)	Lift over drag ratio: $L/D \geq L/D_{baseline}$	Aerodynamics ($@V_{design}$)
G(10)	Wing taper ≥ 0·2	Geometry
G(11)	Take-off ground roll ≤ 438m (1,440ft)	Performance(*@WOT*)
G(12)	Maximum speed (V_{max}) ≥ 60·3ms^{-1}	Performance (*@WOT*)
G(13)	Stall speed (V_{stall}) ≤ 27·8ms^{-1}	Performance (Clean)
G(14)	Service ceiling ≥ 25,000ft	Performance (*@WOT*)
G(15)	Hinge moment equation @ take-off condition	Performance (@low V)
G(16)	Directional stability derivative: $C_{n\beta} \leq 0{\cdot}28$	S&C ($@V_{design}$)
G(17)	Directional stability derivative: $C_{n\beta} \geq 0{\cdot}08$	S&C ($@V_{design}$)

Table 5
Uncertainty variable and parameter selection

	Name	Interval Width	Mean Value
Uncertain Variable	Design speed	± 3ms^{-1}	42ms^{-1}
	Density correction	± 0·02kg/m^3	0
	Design altitude	± 250 m	3,000m
	Payload	± 10 kg	204kg
	Battery weight	±3%	321·25kg
Uncertain Parameter	Battery pack voltage	±10%	600V
	Battery pack capacity	±10%	200Ah
	Battery cell voltage	±1%	3·6V
	Battery cell amperage	±1%	19Amp
	Battery cell weight	±1%	0·107kg
	Propeller efficiency	±5%	0·85

3.5 Optimum UAV results

The electric-powered UAV analysis results based on the Predator A show agree well with the baseline aerodynamic, S&C, weight, and performance data, as shown in Table 6. The endurance was reduced to 4·86 hours for a fully armed payload with a Tenergy Li-$SOCl_2$

https://doi.org/10.1017/S0001924000011313 Published online by Cambridge University Press

battery due to battery technology limitations for the baseline. The Design Explorer Optimisation method [29], which uses the Latin Hyper-cube method to seek an entire design space with 123 design points and a Sequential Quadratic Programming (SQP) method, was applied to determine the electric-powered UAV configurations that corresponded to a possibility index of 1, as shown in Table 6. The possibility index alpha values were calculated from 0 to 1. The alpha value of 1 represents the deterministic optimum results, while the alpha of 0·4 represents the most conservative optimum results when considering the entire uncertainty interval given for a UAV design formulation. However, the optimal UAV results are shown for alpha values from 0·4 to 1 in Table 6. Due to the 17 design variables, 17 constraints, and 11 uncertainty variables, the UAV design formulation has a small feasible region. Therefore, the UAV configuration cannot be optimised for alpha values between 0 and 0·2 because feasible regions could not be found during the optimisation search, as shown in Fig. 7. The most conservative UAV configuration was reached at an alpha value of 0·4, for which the endurance was improved from the baseline 4·86 hours to 5·41 hours. When the possibility index alpha value increased to 1, the UAV endurance also improved and was maximised at 6·55 hours, which corresponded to the deterministic UAV results in Table 6 when all constraints are satisfied. Increasing the possibility index from 0·4 to 1 indicates that certain data are defined in the uncertainty interval. Therefore, the relationship between the endurance and alpha value primarily consists of a compromise with the PBDO concept. The optimal wingspan increased from the baseline value at different possibility indices and was maximised at an alpha value of 1, which corresponded to the deterministic results. The wing tip chord reached a lower bound to improve the aerodynamic characteristics. This value increased the lift to drag ratio at the optimal UAV configuration for different possibility indices, as shown in Table 6. The lift over drag ratio increased from a baseline to different possibility indices and reached a maximum value of 28·61 at the deterministic configuration. The wing weight, empty, and gross weight increased and satisfied the constraints due to the increase in the wingspan and area shown in Table 6.

The optimal UAV configuration performance characteristics, such as the stall speed, maximum speed, take-off, and landing distance, also improved from the baseline value due to the increased wingspan and lift over drag ratio. These characteristics were maximised at the deterministic optimum configuration. All performance constraints satisfied the constraints given in the UAV design formulation. The static stability constraints, including the SM, lateral and directional static derivative coefficients, and pitching moment coefficient were satisfied at the optimal UAV configuration with different possibility indices. The wing sweep, horizontal tail area, and location were adjusted to satisfy the SM and pitching moment coefficient constraints given in the design formulation shown in Table 6. The vertical tail area and location were changed to satisfy the static lateral and directional stability coefficients, as shown in Table 6. The design speed was also considered as an uncertainty variable and reduced from $42 ms^{-1}$ at the baseline to $39·8 ms^{-1}$ at an alpha of 0·4, as shown in Table 6. The design speed was minimised at $34 ms^{-1}$ for the deterministic result. The UAV operated at lower speed, which reduced the battery use during flight and increased the endurance, as shown in Table 6. The design speed reduced linearly with the increase in the possibility index due to uncertainty design speed variable consideration.

https://doi.org/10.1017/S0001924000011313 Published online by Cambridge University Press

Table 6
Electric-powered UAV optimal configurations at different possibility index

		Baseline	α = 0·4 result	α = 0·6 result	α = 0·8 result	α = 1·0 result	Unit
Objective function	**Endurance**	**4·86**	**5·41**	**6·11**	**6·34**	**6·55**	**hours**
Design Variables	Wing span	14·8	16·61	17·98	18·42	18·5	m
	Wing root chord	1·24	1·20	1·21	1·25	1·3	m
	Wing tip chord	0·5	0·40	0·375	0·375	0·375	m
	Wing sweep	5	4·35	4·48	7·23	3·69	°
	Wing dihedral	0	0·00	0·00	0·00	0	°
	Wing *x* location	3·59	4·00	3·50	3·44	3·43	m
	HT span	4	3·84	3·54	3·80	3·53	m
	HT root chord	0·742	0·61	0·83	0·46	0·85	m
	HT tip chord	0·742	0·58	0·59	0·40	0·6	m
	HT sweep	0	5·10	2·05	4·94	1·91	°
	HT *x* location	6·82	7·80	7·23	7·80	7·11	m
	VT span	1·14	1·50	1·50	1·50	1·5	m
	VT root chord	0·742	1·00	1·00	0·93	1	m
	VT tip chord	0·742	0·93	0·50	0·42	0·46	m
	VT LE sweep	45	0·00	13·26	0·00	35·3	°
	VT *x* location	6·82	7·15	6·90	7·30	6·89	m
	Vdesign	42	39·80	38·60	36·50	34	ms^{-1}
Constraints	Wing taper ratio	0·4	0·31	0·30	0·30	0·30	
	Lift over drag ratio	21·3	23·20	25·60	26·10	28·61	
	Maximum speed	76·1	77·80	78·20	78·95	80·83	ms^{-1}
	Stall speed	24·48	24·04	23·11	22·58	22·21	ms^{-1}
	Take-off ground roll	317·75	323·60	325·12	341·20	356·40	m
	Take-off field length	521·29	540·20	550·45	560·40	572·30	m
	Landing distance	400·37	413·12	420·60	425·10	430·4	m
	$C_{l\beta}$	0·0069	–0·030	–0·032	–0·045	–0·091	
	$C_{l\beta}$	0·0055	0·080	0·080	0·080	0·08	
	$C_{m\alpha}$	–0·741	–0·74	–0·76	–0·81	–0·85	
	SM	0·106	0·05	0·089	0·115	0·126	
	Wing weight	91	92·20	93·10	94·50	95·4	kg
	MTOW	1,011·7	1,013·30	1,014·20	1,016·81	1,018·2	kg
	Empty weight	334·7	337·80	339·50	340·78	342·3	kg

The 3D optimal UAV configuration for various possibility indices is shown in Fig. 8. The wingspan was increased from the baseline value to the deterministic optimal configuration. The baseline and optimal configuration of the possibility index values at 0·6 and 1 were validated by ANSYS Fluent 13.

3.6 High fidelity analysis validation

The objective function of the electric-powered UAV maximised the endurance. Therefore, the validation of the lift and drag module is significant to insure the reliability of low fidelity aerodynamics module for the optimum results. The entire baseline optimal UAV configuration

https://doi.org/10.1017/S0001924000011313 Published online by Cambridge University Press

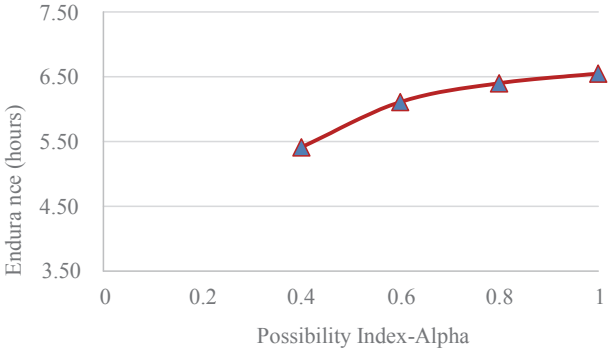


Figure 7. Electric-powered UAV endurance vs Alpha.

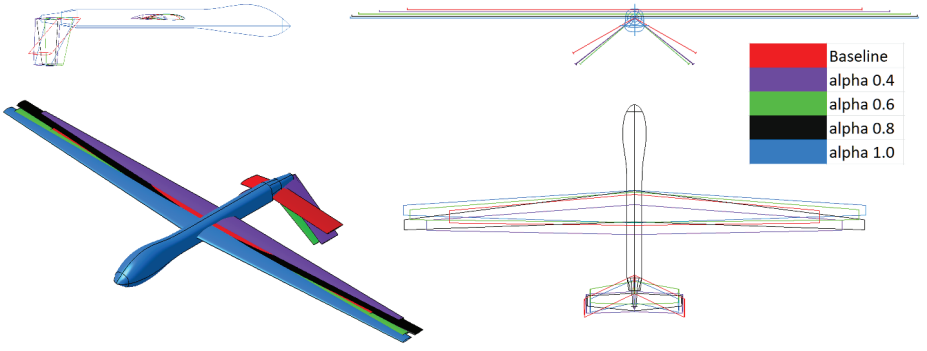


Figure 8. 3D optimal UAV configuration with various possibility index.

was validated by ANSYS Fluent 13 for a baseline and a possibility index values of 0·6 and 1. The meshing topology for the entire electric-powered UAV configuration is shown in Fig. 9. The symmetric model of electric-powered UAV was meshed.

Steady state calculations were used to compute the aerodynamic coefficients and flow field of the entire UAV configuration in ANSYS-Fluent 13. The mesh was modelled using Pointwise[30] grid generation software. Reynolds-Averaged Navier-Stokes (RANS) equations were applied to describe the flow around a UAV Single equation Spalart-Allmaras turbulent model (S-A), which was specifically developed by Spalart and Allmaras for aerospace applications involving wall-bounded flows. This model was used in the current calculation. The model showed a good agreement for boundary layers subjected to adverse pressure gradients.

The flow was investigated around half of the entire UAV configuration because the UAV configuration geometry was symmetric. To precisely calculate the boundary-layer properties, a dense mesh was generated around the UAV configuration. The Y+ value at the wing and tail surface was equal to 1·0 and greater than 1·0 at the body surface. Applying a Y+ value less than 1·0 at the body surface leads to high aspect ratio cells and mesh geometryproblems. A dense mesh with 2·6 grid points was used to precisely predict the aerodynamic characteristics of the entire UAV configuration. The grid system is shown in Fig. 9. Maximum residuals of the velocity components, energy and continuity of less than 10^{-4} w were selected as the convergence criteria.

https://doi.org/10.1017/S0001924000011313 Published online by Cambridge University Press

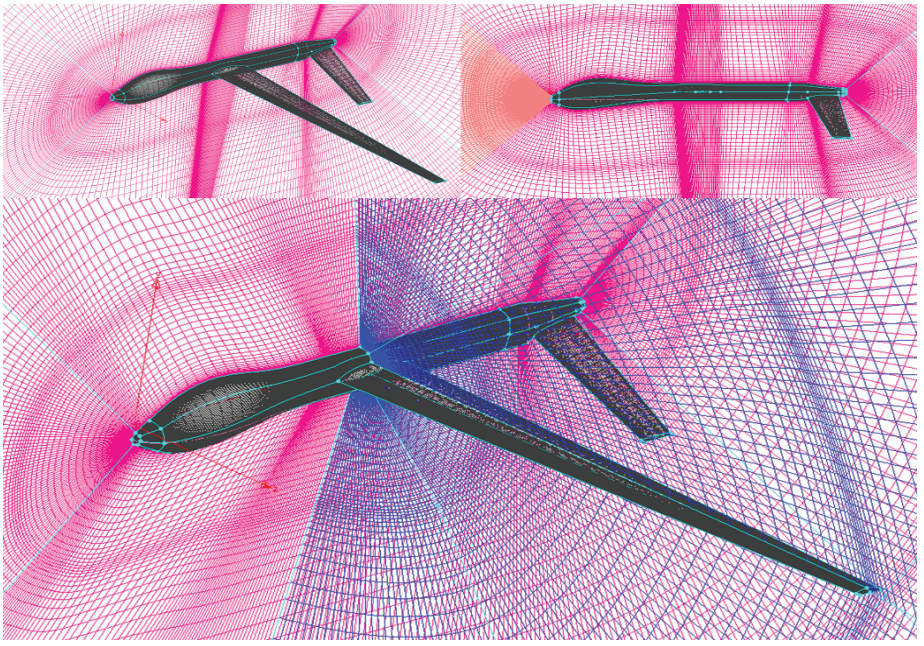


Figure 9. Entire electric-powered UAV grid system.

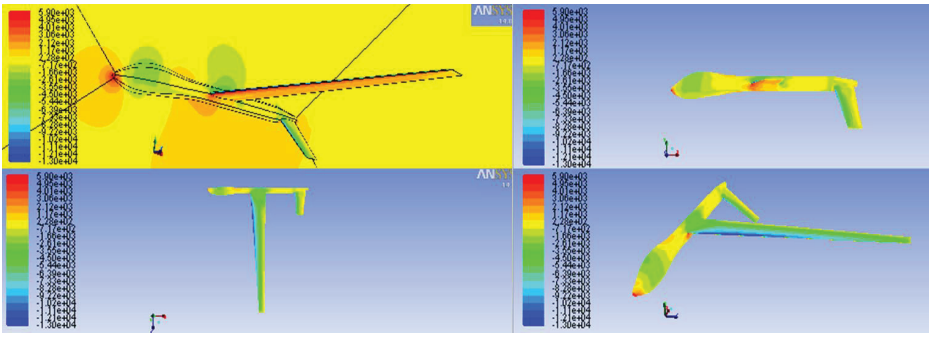


Figure 10. Pressure distribution for the entire UAV configuration at cruise condition.

The pressure distribution on the entire UAV configuration is shown in Fig. 10. The low speed cruise condition was analysed at 42ms^{-1}, 38·6ms^{-1}, and 34ms^{-1} for the baseline, a possibility index of 0·6, and a possibility index of 1 configuration, respectively in Table 6. The highest pressure regions appeared on the nose of the UAV, the lower wing, lower wing, and lower horizontal tail surface, as shown in Fig. 10. The lowest pressure region was on the upper wing surface, due to a very long wingspan and low speed. These conditions produce a higher lift force on the wing and a higher lift-to-drag ratio. The endurance was improved. The pressure distribution was higher near the upper wing tip region due to the induced effect at the outboard wing. Therefore, the RANS solver captured the UAV aerodynamic characteristics well. In addition, the turbulence model was applied to the current analysis. However, the flow was a low speed regime and mostly laminar in the wing, tail, and fuselage. Hence, the drag coefficient was over-estimated due to the turbulence

https://doi.org/10.1017/S0001924000011313 Published online by Cambridge University Press

model. The baseline and a possibility index values of 0·6 and 1 configurations were calculated at cruise condition. The cruise lift coefficient comparison between high fidelity analysis and iUAV analysis tool at three different configurations are presented in Table 7. The results show very good agreement with the high fidelity analysis results at the maximum error of 4·08% comparing with the high fidelity analysis results. Therefore, the accuracy of results was verified to demonstrate the effectiveness of the proposed process.

Table 7
The UAV high fidelity analysis validations comparison

	Lift coefficient (iUAV tool)	Lift coefficient (ANSYS Fluent 13)	Difference (%)
Baseline configuration	0·525	0·513	2·35
Alpha = 0·6 configuration	0·474	0·46	2·95
Alpha = 1 configuration	0·490	0·47	4·08

4.0 CONCLUSION

A possibility-based multidisciplinary optimisation for an electric-powered UAV design was successfully presented and demonstrated by resizing a Predator A configuration with uncertainty considerations in the design formulation. The optimal electric-powered UAV results show a very good agreement and trend when increasing the possibility index from 0·4 to 1. The optimal electric-powered UAV configuration, which increased when increasing the possibility index from 0·4 to 0·8, yielded more conservative results compared with the deterministic results. The optimal configuration with uncertainty considerations is more reliable than the deterministic optimal result.

The electric-powered system was investigated to replace a piston engine system and to generate a propulsion analysis based on the blade element theory. The electric-powered system and propeller analysis results were created to analyse the electric-powered UAV performance. The uncertainty considerations for the battery voltage, capacity, and weight were simulated to make the electric-powered UAV design problem more realistic. This approach resulted in a more conservative configuration with different possibility index values.

The accuracy of a baseline and two optimal electric-powered UAV configuration at possibility index values of 0·6 and 1 was verified by the high fidelity analysis ANSYS Fluent 13 to demonstrate the effectiveness and feasibility of the proposed method with maximum error of 4·08 percent.

ACKNOWLEDGEMENTS

This paper was supported by Konkuk University in 2013 and Konkuk University Brain Pool 2015. The authors also would like to thank Dr Daniel Neufeld for his contribution on iPBDO program and Jimin Kim. The corresponding author email: jwlee@konkuk.ac.kr.

REFERENCES

1. SOBIESZCZANSKI-SOBIESKI, J. and HAFTKA, R.T. Multidisciplinary aerospace design optimization: survey of recent developments, *Structural and Multidisciplinary Optimization*, 1997, **14**, (1), pp 1–23.
2. MAVRIS, D.N. BANDTE, O. and DELAURENTIS, D.A. Robust Design Simulation: A Probabilistic Approach to Multidisciplinary Design, *J Aircr*, 1999, **36**, (1), pp 298–307.

https://doi.org/10.1017/S0001924000011313 Published online by Cambridge University Press

3. RAO, S.S. and CAO, L. Optimum Design of Mechanical Systems Involving Interval Parameters, *ASME J*, 2002, **124**, (3), pp 465–472.
4. TAGUCHI, T., YOKOTA, T. and GEN, M. Reliability optimal design problem with interval coefficients using hybrid genetic algorithms, *Computers & industrial engineering*, 1998, **35**, (1), pp 373–376.
5. TAGUCHI, G. and RAFANELLI, A.J. Taguchi on Robust Technology Development: Bringing Quality Engineering Upstream, 1994.
6. PARK, G.-J. LEE, T.H., LEE, K. H. and HWANG, K.-H., Robust design: An overview, *AIAA J*, 2006, **44**, (1), pp 181–191.
7. CHEN, W., GARIMELLA, R. and MICHELENA, N. robust design for improved vehicle handling under a range of maneuver conditions, *Engineering Optimization*, February 2001, **33**, (3), pp 303–326.
8. NEUFELD, D., JOON, C. and KAMRAN, B. Aircraft conceptual design optimization considering fidelity uncertainties, *J Aircr*, October 2011, **48**, (5), pp 1602–1613.
9. NEUFELD, D., BEHDINAN, K. and CHUNG, J. Aircraft wing box optimization considering uncertainty in surrogate models, July 2010, pp 745–753.
10. OH, S., LEE, G.J. and NAH, S.-H. Aerodynamic Design and Aviation Procedure Considering Global Warming, in KSASS, 2010.
11. Selection of Electronic Motors for Aerospace Applications, NASA, Marshall Space Flight Center, PRACTICE NO.PD-ED-1229.
12. Chapter 1. Electric vehicles for aerospace applications.
13. FEHRENBACHER, J., STANLEY, D.L. JOHNSON, M.E. and HONCHELL, J. Electric Motor & Power Source Selection for Small Aircraft Propulsion, Purdue University, USA, 2011.
14. HARMON, F.G., FRANK, A.A. and CHATTOT, J. Conceptual design and simulation of a small hybrid-electric unmanned, aerial vehicle, *J Aircr*, 2006, **43**, (5), pp 1490-1498.
15. NGUYEN, N.-V., CHOI, S.-M., KIM,W.-S., LEE, J.-W., KIM, S., NEUFELD, D and BYUN, Y.-H. Multidisciplinary unmanned combat air vehicle system design using multi-fidelity model, *Aerospace Science and Technology*, **26**, 2013, pp 200-210.
16. DRELA, M. and YOUNGREN, H. *Athena Vortex Lattice*, 2008.
17. RAYMER, D. *Aircraft Design: A Conceptual Approach*, 4th ed, AIAA, 2006.
18. ROSKAM, J. *Airplane Design Parts I through VIII*, 2nd ed. Darcorporation, 2003.
19. GUNDLACH, J. *Designing Unmanned Aircraft Systems: A Comprehensive Approach*, AIAA Education Series, 2012.
20. LOWRY, J.T. *Performance of Light Aircraft*, AIAA education series, 1999.
21. DRELA, M. XFoil Subsonic Airfoil Development System. Online. Available: http://web.mit.edu/drela/Public/web/xfoil/. Accessed: 2 March 2013.
22. NHU VAN NGUYEN, N.V., LEE, D., PARK, H.-U., TYAN, M. and LEE, J.W. A Multidisciplinary Robust, Optimization Framework for UAV Conceptual Design, *Aeronaut J*, February 2014, **118**, (1199), pp 123-142.
23. MÖLLER, B and BEER, M. Engineering computation under uncertainty-capabilities of non-traditional models, *Computers & Structures*, 2008, **86**, (10), pp 1024–1041.
24. PHAM, T.D. and VALLIAPPAN, S. Constructing the Membership Function of a Fuzzy Set with Objective and Subjective Information, *Computer-Aided Civil and Infrastructure Engineering*, 2008, **8**, (1), pp 75–82.
25. HE, L.P., HUANG, H.Z., DU, L., ZHANG, X.-D. and MIAO, Q. A Review of Possibilistic Approaches to Reliability Analysis and Optimization in Engineering Design – Springer, Human-Computer Interaction, HCI Applications and Services, 2007, **4553**, pp 1075–1084.
26. NEUFELD, D., NHU VAN, N.,LEE, J.-W. and KIM, S. A Multidisciplinary Possibilistic Approach to Light Aircraft Conceptual Design, AIAA 2012-1434, 8th MDO Specialists, Hawaii, USA, April 2012.
27. FLUENT 6.0 User's Guide. Available: http://202.118.250·111:8080/fluent/Fluent60_help/html/ug/main_pre.htm. 28. ANSYS Fluent 13, ANSYS, Inc., www.ansys.com.
29. PHX ModelCenter® | Phoenix Integration. Online.. Available: http://www.phoenix-int.com/software/phx – modelcenter.php.
30. Pointwise 16 User manual: http://www.pointwise.com/

https://doi.org/10.1017/S0001924000011313 Published online by Cambridge University Press